PCCP

Molecular dynamics simulations of the structure of the graphene-ionic liquid/alkali salt mixtures interface

Journal:	*Physical Chemistry Chemical Physics*
Manuscript ID:	CP-ART-03-2014-000918.R1
Article Type:	Paper
Date Submitted by the Author:	14-May-2014

Complete List of Authors:	Mendez-Morales, Trinidad; University of Santiago de Compostela, Condensed Matter Physics Carrete, Jesus; CEA - French Atomic Energy Commission, DRT/LITEN/DTNM/LCRE Pérez, Martín; Universidade de Vigo, Física Aplicada Cabeza, Oscar; Universidade de A Coruña, Física Javier Gallego, Luis; Universidad de Santiago de Compostela, Física de la Materia Condensada Lynden-Bell, Ruth; University of Cambridge, Department of Chemistry Varela, Luis Miguel; University of Santiago de Compostela, Condensed Matter Physics

SCHOLARONE™
Manuscripts

Physical Chemistry Chemical Physics
CREATED USING THE RSC LaTeX PCCP ARTICLE TEMPLATE – SEE www.rsc.org/electronicfiles FOR DETAILS
ARTICLE TYPE www. rsc.org/xxxxxx | XXXXXXXX

Molecular dynamics simulations of the structure of the graphene-ionic liquid/alkali salt mixtures interface

Trinidad Méndez-Morales,[a] Jesús Carrete,[a,b] Martín Pérez-Rodríguez,[c] Óscar Cabeza,[d] Luis J. Gallego,[a] Ruth M. Lynden-Bell [e] and Luis M. Varela*[a]

Received Xth XXXXXXXXXX 20XX, Accepted Xth XXXXXXXXX 20XX
First published on the web Xth XXXXXXXXXX 200X
DOI: 10.1039/b000000x

We performed molecular dynamics simulations of mixtures of 1-butyl-3-methylimidazolium tetrafluoroborate with lithium tetrafluoroborate and potassium tetrafluoroborate between two charged and uncharged graphene walls, in order to analyze the structure of the well-known formation of layers that takes place on liquids under confinement. For this purpose, we studied the molecular density profiles, free energy profiles for bringing lithium and potassium cations from the bulk mixture to the graphene wall and the orientational distributions of imidazolium rings within the first adsorbed layer as a function of salt concentration and electrode potential. The charge densities in the electrodes were chosen to be zero and ± 1 e/nm^2, and the salt molar percentages were $\%_{salt}$= 0, 10 and 25. We found that the layered structure extends up to $1-2$ nm, where the bulk behaviour is recovered. In addition, whereas for the neutral surface the layers are composed of both ionic species, increasing the electrode potential, the structure changes to alternating cationic and anionic layers leading to an overcompensation of the charge of the previous layer. We also calculated the distribution of angles of imidazolium rings near neutral and charged graphene walls, finding a limited influence of the added salt. In addition, the average tilt of the imidazolium ring within the first layer goes from 36° with respect to a normal vector to the uncharged graphene wall to 62° in the presence of charged walls. The free energy profiles revealed that lithium and potassium ions are adsorbed on the negative surface only for the highest amount of salt, since the free energy barriers for approaching this electrode are considerably higher than k_BT.

1 Introduction

During the last decades there has been an increasing interest in room temperature ionic liquids (RTILs), salts composed entirely of ions with melting points below 100 °C, mainly due to their fascinating physical and chemical properties and their potential use in several fields. These key properties can be controlled with the appropiate selection of cations and anions, which contributes to their reputation as "green solvents" and makes them promising candidates for a great number of applications, ranging from biological uses, synthesis and catalysis, to lubrication or heat storage. In particular, they are known to show high ionic conductivity, low vapour pressure that makes them practically non-flammable and wide electrochemical window; which provide them with a huge potential in electrochemical applications such as supercapacitors, solar cells or lithium batteries, among others.

Regarding electrochemical devices, the choice of the electrolyte employed when producing a lithium battery is of crucial importance and the possibility of improving not only the efficiency, but also the safety of these devices by applying ILs as electrolytes, has led to a vast number of studies during the last few years.[1–7] Since ILs are practically non electroactive, any attempt to use them as electrolytes in lithium batteries requires mixing of the IL with a suitable lithium salt, resulting in a mixture of three or four ions. At this point, the main aspects that need particular attention for optimum battery operation are: firstly, a detailed picture of the solvation processes of lithium ions in the bulk IL and, secondly, the influence of these lithium salts on the well-known solvation layers formed at the electrode/IL interface. Although both aspects play a fundamental role in the performance of lithium batteries, they still remain as open questions and a deeper understanding is required.

Concerning lithium environment in bulk IL mixtures, very few publications have focused on the structural and dynamic properties of lithium salts doping aprotic ionic liquids (AILs) (See Ref. 8 and references cited therein) and, to our knowl-

[a] *Grupo de Nanomateriais e Materia Branda, Departamento de Física da Materia Condensada, Universidade de Santiago de Compostela, Campus Vida s/n E-15782, Santiago de Compostela, Spain*
[b] *CEA, DRT, 38054 Grenoble, France*
[c] *Departamento de Física Aplicada, Universidade de Vigo, Lagoas-Marcosende s/n E-36310, Vigo, Spain*
[d] *Facultade de Ciencias, Universidade da Coruña, Campus A Zapateira s/n E-15008, A Coruña, Spain*
[e] *University of Cambridge, University Chemical Laboratory, Lensfield Road, Cambridge, UK CB2 1EW*
* *E-mail: luismiguel.varela@usc.es*

edge, only two papers have been reported for protic ionic liquids (PILs).[9,10]

On the other hand, due to the fact that understanding the influence of the nature of the IL ions, temperature and applied electrode potential on the properties of the electric double layer is of paramount importance for theoretical and practical purposes, as indicated in some influential experimental[11] and computational[12] results, much theoretical, computational and experimental research devoted to this issue is needed. In spite of this, it must be said that even though great progress has been made towards a fundamental understanding of the behaviour of ILs at charged interfaces, this question has been much less extensively studied than bulk properties. In this case, the analysis of the differential capacitance (DC) as a function of the electrode potential has been regarded as a helpful source of information about the electric double layer behaviour and, up to now, many experimental[13–16] and computational[17–26] studies have reported bell-shaped or camel-shaped DC curves.

From the theoretical point of view, Kornyshev stressed[27] that the Gouy-Champman-Stern theory could not be applied to these dense ionic systems, in which the effects of ionic correlations and overscreening are important.[28] The author proposed a mean-field theory (MFT) to interpret the potential dependence of the double-layer capacitance at a planar metal/IL interface. However, last year Gebbie *et al.*[29] reported a controversial picture in which ILs would behave as dilute electrolyte solutions due to the existence of a very limited amount of unpaired ions in ILs. Their reported results for the force between colloidal particles immersed in bulk ILs was interpreted as showing that the screening of charged surfaces by ILs takes place through the formation of both bound (Stern) and diffuse electric double layers, where the latter is composed of effectively dissociated ions. Hence, the essentials of screening in ILs are still in need of more stable foundations.

In addition, the arrangement and the orientations of the ions at the IL/electrode interface, with a multiple layer organization at the surface, have been experimentally investigated by means of atomic force microscopy (AFM),[30–32] scanning tunneling microscope (STM),[31,33,34] a surface force apparatus (SFA),[35,36] X-ray reflectivity[37] and X-ray spectroscopy studies.[38] By contrast, several groups concluded that some ILs do not show interfacial layering, but only a single ion layer of enhanced electron density.[39–41]

Since the formation of the electric double layers is a highly complicated phenomena, experimental mesurements can be complemented by atomistic simulations in order to shed some light into the structure of the electrode/IL interface. In addition, due to their lower cost as compared to experimental research, computer simulations are an essential tool for performing systematic studies of ILs and designing new and improved materials. Thus, many groups have focused up to now on the interface behaviour of IL/solid systems from a computational perspective,[12,42–48] molecular dynamics (MD) being the most widely employed technique. For example, Pinilla *et al.*[49,50] employed MD simulations to study the behaviour of 1,3-dimethylimidazolium chloride ([DMIM][Cl]) confined between two charged ($\pm 0.12\ \mathrm{e}/\mathrm{nm}^2$) and neutral parallel walls. Their simulations revealed a clear structure of layers with a high-density peak at the proximities of the walls followed by weaker oscillations toward the bulk system, as well as a rearrangement of the ions with increasing field strength. In addition, they determined that cations at the interface tend to orient their rings tilted around 70° with respect to the surface. More recently, Lynden-Bell *et al.*[51,52] investigated the properties of [DMIM][Cl] near charged graphene surfaces. They also reported the formation of several alternating layers of cations and anions with ion densities higher than in the bulk even at the non-charged electrode surface. Regarding the orientation of the ions, the authors found that, at the neutral electrode, the preferential orientation of the cations is parallel to the surface, whereas near the negative electrode some of them tend to be perpendicular to the surface. They concluded that the IL provides excellent electrostatic screening at distances longer than $1-2$ nm.

In spite of the number of studies that have explored the electric double layer structure in ILs using probes, to our knowledge only one publication has been reported focusing on IL/lithium salt mixtures near interfaces. In this case, Smith *et al.*[53] performed atomistic MD simulations of a lithium iron phosphate ($LiFePO_4$) surface in contact with a mixture of 1-ethyl-3-methylimidazolium bis(fluorosulfonyl)amide ([EMIM][FSI]) with a 22.6% of lithium bis(fluorosulfonyl)amide (LiFSI). They observed a free energy barrier for bringing $[Li]^+$ cations from the bulk system to the surface of around 16 kJ/mol.

In this work we performed MD simulations of mixtures of 1-butyl-3-methylimidazolium tetrafluoroborate ([BMIM][BF_4]) (chosen by electrochemical interest and because its bulk properties had been analyzed previously[8]) with lithium tetrafluoroborate ($LiBF_4$) and potassium tetrafluoroborate (KBF_4) confined between two parallel graphene surfaces, with the aim of gaining some insight into the structure of IL/alkali salts electrolytes at the proximities of charged and neutral electrodes. Molecular density profiles, free energy profiles for bringing $[Li]^+$ and $[K]^+$ cations from the bulk mixture to the graphene wall and imidazolium orientational distributions within the first adsorbed layer were analyzed as a function of salt concentration and electrode potential.

The outline of this paper is as follows. In section 2, we provide a detailed account of the simulation method. In section 3, we present and discuss the results obtained and concluding remarks are offered in section 4.

This journal is © The Royal Society of Chemistry [year]

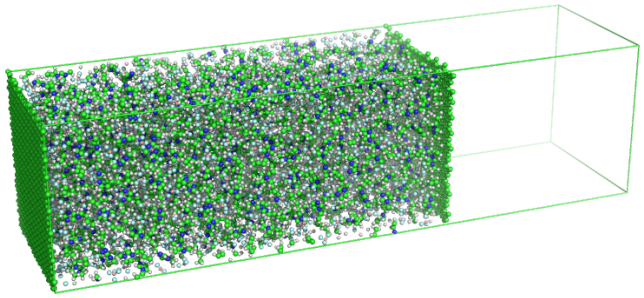

Fig. 1 Schematic representation of the simulation box for the pure IL along the Z direction. The liquid is confined between two walls separated by 10.48 nm, and whose sides measure 4.2 nm. The system is periodically repeated every 16 nm in the Z direction.

2 Simulation details

We performed MD simulations of [BMIM][BF_4] doped with either $LiBF_4$ or KBF_4 enclosed between two flat graphene walls using the GROMACS 4.5.4 package.[54] In order to avoid the system being "trapped" in a local minimum due to the well-known high viscosity of ILs, the temperature investigated was $T = 450$ K, and the molar percentages of salt considered in the mixtures were $\%_{salt}$= 0, 10 and 25. The number of lithium/potassium salt molecules was calculated for each situation by considering each ionic pair as a single unit in the calculation of mole fractions.

The fixed graphene walls had charges and a Lennard-Jones (LJ) center on each carbon seat and they were built with the help of the Visual Molecular Dynamics (VMD) package.[55] The charges on the carbon atoms of the graphene sheets were chosen to give wall charge densities of $+1$ e/nm^2 and -1 e/nm^2 in the left and right electrodes, respectively (and zero in the uncharged case). Their LJ parameters were $\sigma_C = 3.55 \cdot 10^{-1}$ nm and $\varepsilon_C = 2.9288 \cdot 10^{-1}$ kJ/mol. The graphene sheets were placed parallel to the XY-plane in such a way that one electrode was kept at $Z = 0$ and the other one was located at positive values of Z at the distance needed to obtain the bulk density in the middle of the rectangular box used to emulate a semi-infinite slab geometry. All three coordinates of these carbon atoms were frozen at their initial values and the electrodes were held rigid with a carbon bond length of $l_{CC} = 0.142$ nm. Periodic boundary conditions were applied in all directions and the graphene electrodes were considered as periodic molecules in order to couple to themselves through the periodic boundary conditions. A slab of vacuum was left outside the confining sheets for avoiding artificial influence from periodic images, as shown in Fig. 1.

We employed the OPLS-AA force field in order to carry out the parametrization of the ions. This all-atom version of the OPLS force field, in which every hydrogen atom bonded to carbon is modeled explicitly, was developed by Jorgensen[56] for different organic liquids. The functional form of the OPLS force field takes the standard form

$$\begin{aligned} E = &\sum_i K_{b,i}\,[r_i - r_{0,i}]^2 + \sum_i K_{b,i}\,[\theta_i - \theta_{0,i}]^2 + \\ &+ \sum_i \left[\frac{1}{2} V_{1,i}(1+\cos(\varphi_i)) + \frac{1}{2} V_{2,i}(1+\cos(2\varphi_i)) + \right. \\ &\left. + \frac{1}{2} V_{3,i}(1+\cos(3\varphi_i)) + \frac{1}{2} V_{4,i}(1+\cos(4\varphi_i)) \right] + \\ &+ \sum_i \sum_{j<i} \left\{ \frac{1}{4\pi\varepsilon_0} \frac{q_i q_j e^2}{r_{ij}} + 4\varepsilon_{ij} \left[\left(\frac{\sigma_{ij}}{r_{ij}} \right)^{12} - \left(\frac{\sigma_{ij}}{r_{ij}} \right)^{6} \right] \right\}, \quad (1) \end{aligned}$$

which includes intramolecular interactions such as bond stretching, angle bending, dihedral torsion, as well as van der Waals and Coulombic interactions. The parameters employed in eq. (1) are the force constants K, the nominal values r_0 and θ_0, the Fourier coefficients V, and the partial atomic charges q fixed on each atom center. σ_{ij} and ε_{ij} represent the LJ radii and potential well depths, respectively, which are obtained from parameters for each type of atom by using geometric combination rules $\varepsilon_{ij} = \sqrt{\varepsilon_{ii}\varepsilon_{jj}}$ and $\sigma_{ij} = \sqrt{\sigma_{ii}\sigma_{jj}}$. The imidazolium cation was modeled by using the all-atom representation of the CH_2 and CH_3 groups in the alkyl chain, as well as that of the methyl group attached to the imidazolium ring, and its parameters were assigned according to the values reported by Sambasivarao and Acevedo;[57] while lithium and potassium cations were modeled by a single site of charge $+1$ and LJ parameters taken directly from GROMACS database. As for the anion, $[BF_4]^-$ was modelled as a set of 5 sites with partial charges of $+1.776$ for the boron atom and -0.544 for the fluorine atoms.[58] The electronic polarizability for both the graphene walls and the electrolyte was not taken into account in our study, since although polarizability has been found to have a deep impact on dynamic properties of ILs, Yan *et al.*[59] showed that the major structural properties of the IL/vacuum interface for both polarizable and non polarizable models were similar. Long-range electrostatic interactions were treated by using the Particle Mesh Ewald (PME)[60] method with a FFT grid spacing of 12 nm, a 1.1 nm cut-off distance for the real space sum and cubic interpolation; together with Yeh-Berkowitz corrections for our slab geometry.[61,62] A cut-off radius of 1.1 nm was used for LJ interactions, and a neighbor updated for the nonbonded interactions was made up to this same distance from the central ion and was updated every ten simulation steps. The Linear Constraint Solver (LINCS) algorithm[63,64] with a fourth-order expansion of the constraint coupling matrix was used to fix all the bond lengths.

Initial configurations were relaxed for 10^6 steps using a conjugate gradients algorithm in order to remove bad contacts resulting from the initial random configuration of ions.

The maximum step size and the tolerance were set to 0.01 nm and 1 kJ/(nm · mol), respectively. For each molar percentage of salt, the system was heated during 100 ps from 450 K to 1000 K in the NVT ensemble, followed by a run of 100 ps; cooling it gradually to 450 K during further 100 ps. Following annealing, each mixture was equilibrated for 30 ns at 450 K and the resultant configurations were taken as the initial configurations for the production runs. The time step of the simulations was 2 fs. The temperature was controlled by using the V-rescale thermostat.[65] Cations and anions were separated in two (or three) baths with temperature coupling constants of 0.1 ps. The results of an additional 10 ns–long simulations in the NVT ensemble were used for obtaining structural information about the systems.

3 Results and discussion

In order to shed some light on the structure of the electric double layer at the interface between ILs/alkali salts mixtures and planar electrodes, Figs. 2 and 3 show, as a function of the distance from the surface, the number density of $[BMIM]^+$ and $[BF_4]^-$ ions near positively (a), negatively (b) and neutrally (c) charged graphene walls for mixtures of $[BMIM][BF_4]$ with $LiBF_4$ and KBF_4, respectively. For this calculations, the positions of the imidazolium cations and tetrafluoroborate anions were computed by considering the carbon atom between the two nitrogens of the imidazolium ring (C2) and the boron atom (B1), respectively. The density profiles for $[Li]^+$ and $[K]^+$ cations were not included since their heights are much lower than those of the ions of the IL, but the positions of their peaks can be inferred from the free energy profiles shown in Fig. 6 below. One remarkable feature shown in Figs. 2.c and 3.c is that, even in the absence of an applied field, the graphene surfaces have an effect on the structure of the liquid. The formation of layers near a neutral graphene wall can be clearly observed in both systems, in which the density of the mixture is much higher than in the bulk. These oscillations of the density in the interfacial area are progressively damped out until values for bulk mixtures are recovered at around 1.5 nm within three layers from the surface. Such layering behaviour has been reported previously in several computational studies.[42–47,49–52] In addition, the layers of the dense region are composed of both ionic species of the IL, $[BMIM]^+$ cations and $[BF_4]^-$ anions, with the presence of imidazoliums approaching slightly closer to the wall and a larger local density of the tetrafluoroborates, probably due to their smaller size. However, there are neither $[Li]^+$ nor $[K]^+$ cations in the first contact layer at any amount of salt (they are firstly located at 0.7 nm); thus, the concentration of adsorbed lithiums and potassiums is zero in contact with neutral graphene.

The highly inhomogeneous layering of the IL in the neighborhood of the graphene electrode is also observed for charged

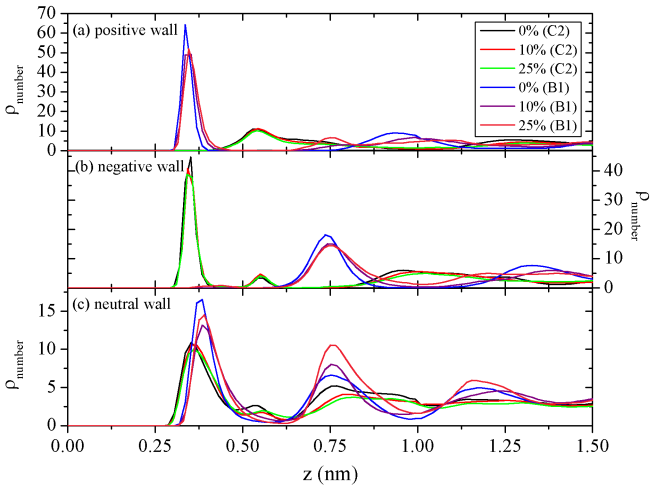

Fig. 2 Number density (in nm^{-3}) for the $[BMIM]^+$, (C2), and $[BF_4]^-$, (B1), ions near positive (a), negative (b) and neutral (c) as a function of the distance to the graphene walls in mixtures of $[BMIM][BF_4]$ with $LiBF_4$.

electrodes. Besides, the surface charge induces molecular reorganization. In comparison with the uncharged surface, the first layer slightly changes its position and moves towards the graphene wall, but its height considerably increases. Moreover, this first peak is composed only of cations in the proximities of the negatively charged electrode ($-1\,e/nm^2$) and, in the same way, composed only of anions in the vicinities of the positively charged surface ($+1\,e/nm^2$). For the latter, the local density is much higher than that of cations near the negative wall, since the first layer can accommodate more tetrafluoroborates due to their smaller size. However, it seems that they do not approach the electrode more than the imidazoliums do. As a result, there are neither adsorbed $[BMIM]^+$ cations on the positive wall nor $[BF_4]^-$ anions adsorbed on the negative surface, and it also results in positive and negative charge densities near the negative and the positive electrode, respectively. This excess of positive/negative charge that overcompensates the electrode charge attracts ions of the opposite ionic species, giving place to the formation of a lower second peak of negative/positive density, respectively. Again, this second layer that overcompensates the charge on the first layer attracts another layer with opposite charge density and so on, until the bulk behavior is reached and all the oscillations are completely smoothed out. In this case, the alternating layers of cations and anions persist up to approximately 2.0 nm for both electrodes and the region where oscillations take place comprises 5 layers. It can be seen that the addition of salt has little effect on the $[BMIM]^+$ and $[BF_4]^-$ density profiles near both charged and uncharged electrodes. On the other hand, as can be seen in Fig. 6 below, near the positively charged surface (Figs.

This journal is © The Royal Society of Chemistry [year]

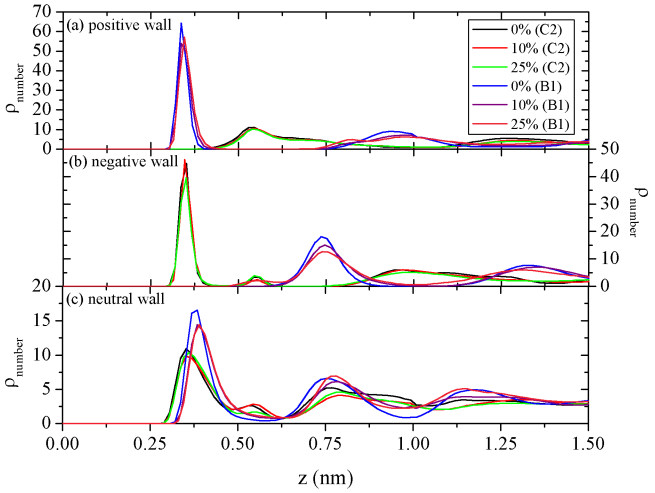

Fig. 3 Number density (in nm^{-3}) for the $[BMIM]^+$, (C2), and $[BF_4]^-$, (B1), ions near positive (a), negative (b) and neutral (c) as a function of the distance to graphene walls in mixtures of $[BMIM][BF_4]$ with KBF_4.

2.a and 3.a) lithium and potassium cations are found at 0.47 and 0.49 nm respectively, between the first anionic layer and the second cationic layer, whereas the behaviour in the vicinities of the negatively charged electrode (Figs. 2.b and 3.b) is slightly different. In this case, for the lowest concentration of salt, 10%, $[Li]^+$ and $[K]^+$ cations are located at around 0.9 nm in the third cationic layer. This shows that the formation of the previously reported anionic aggregates that lithium and potassium form with the anions in their first solvation shell[8,10] is not avoided by the electrode potential or the presence of the surfaces, and it has the greatest impact on the organization of these cations. The picture slightly changes for the highest simulated amount of salt, 25%, for which both lithium and potassium cations approach the negative graphene surface up to 0.21 nm and 0.28 nm, respectively. Those distances are closer to the negative electrode than the first cationic layer, meaning that for lithium/potassium cations to be adsorbed on the graphene wall a considerable amount of salt must be added to the IL, which has a great importance for redox processes.

This behaviour can be clearly observed in Fig. 4, in which we show the structure of the electric double layer near the negative graphene wall for mixtures of $[BMIM][BF_4]$ with a 25% of $LiBF_4$ (left) and KBF_4 (right). It can be observed that, in both cases, the first layer consists of a dense layer of imidazolium cations that overcompensates the wall charge. This first layer is then followed by a second layer of tetrafluoroborate anions due to overcompensations of the charge in the previous layer. Even though the greatest amount of $[Li]^+$ and $[K]^+$ cations is found in the third cationic layer, some of them are able to approach the wall more closely than any other ionic

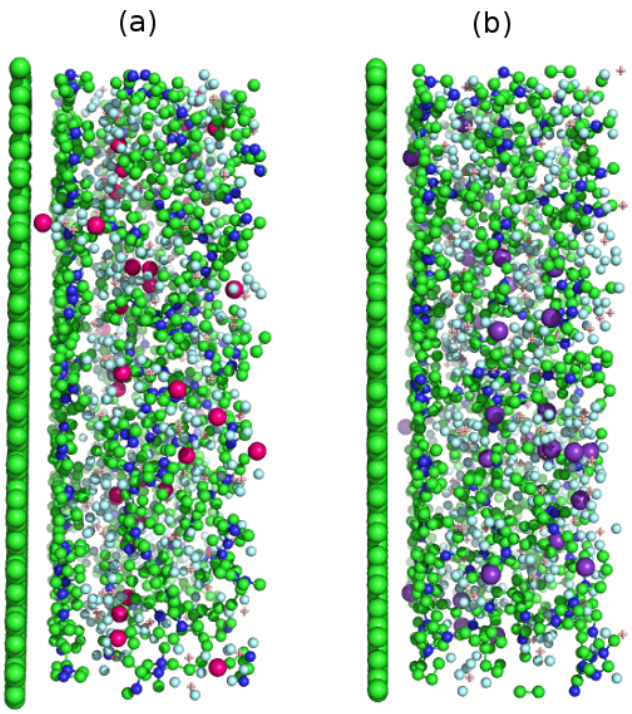

Fig. 4 Snapshots of the structural organization of the ions near negatively charged graphene walls from simulations of $[BMIM][BF_4]$ doped with a 25% of $LiBF_4$ (a) and a 25% KBF_4 (b). The relative size of lithium (dark pink) and potassium (violet) atoms has been exaggerated for the purpose of clarity. Colour coding for the rest of the atoms is as follows: green, carbons; dark blue, nitrogens; light blue, fluorines; and light pink, borons. Hydrogens have been removed for the purpose of clarity.

species for this concentration of salt.

Taking all this information into account, we considered the orientations of imidazolium cations in the first layer of cations in order to know more details of the electric double layer in this kind of systems. The orientational distribution of the ring can be analysed in terms of the angle θ between the vector normal to the walls (parallel to the Z-axis) and a vector normal to the imidazolium ring. In Fig. 5 we plot the probability distribution functions for the ring orientations as a function of $|\cos\theta|$. Note that positive and negative values of $\cos\theta$ are equally likely as the ring is flat and that a uniform distribution of orientations in space would give a flat distribution as a function of $\cos\theta$. Fig. 5 shows the distributions in the first layers of cations near (a) positively charged walls (up to 1.0 nm), (b) negatively charged walls (up to 0.45 nm) and (c) neutral walls (up to 0.65 nm). In addition, in Table 1 we include the average values of $\cos^2\theta$ for the $[BMIM]^+$ cations in the first cation layer near the walls. The results show that the average angle between the normal to ring is about 36° with the

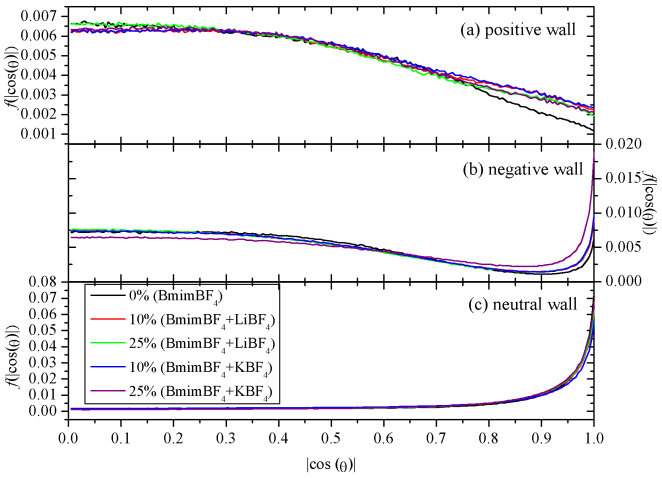

Fig. 5 Probability distribution of $|\cos\theta|$ for the $[BMIM]^+$ cations in the first layer near positively (a), negatively (b) and neutrally (c) charged graphene walls for mixtures of [BMIM][BF_4] with $LiBF_4$ and KBF_4.

normal vector to the neutral wall. Charging the walls results in a new average angle of 62° ring of the cation and both positive and negative walls. These results are in good agreement with those reported by Baldelli near charged IL-metal interface from *SFG* spectra.[40]

We observe in Fig. 5 that at uncharged electrodes the most probable configuration for imidazolium rings is to lie nearly flat on the surface, although there exist a continuous distribution of orientations extending even to orientations perpendicular to the wall. The influence of the added salt in this distribution is almost negligible for uncharged walls. However, charging the wall leads to new configurations for the rings. Near the positively charged wall, the most probable configuration of the $[BMIM]^+$ rings is that in which they are normal to the wall, but there is a broad range of orientations with the probability distribution decaying smoothly to include configurations in which the rings lie flat against the charged surface. In this case, added salt increases the dispersion of the distribution function and chains laying flat to the charged electrode are more likely. On the other hand, near the negatively charged electrode, although a significant fraction of the rings lie flat on the surface, there is a large region of almost constant probability extending form 66° to 90°. Moreover, low-angle orientations are scarcely probable as indicated by the minima of $f(|\cos\theta|)$ near $|\cos\theta| = 0.9$. These minima are displaced towards higher angles with salt addition, and more ions are allowed to lie flat to the interface in these circumstances.

Finally, in Fig. 6 we determined the free energy profiles for bringing a lithium or potassium cation from the bulk to the graphene electrode by

	$<\cos^2\theta>$		
	neutral	$+1\ e/nm^2$	$-1\ e/nm^2$
0.0 %	0.68	0.24	0.20
10.0 %-$LiBF_4$	0.67	0.23	0.22
25.0 %-$LiBF_4$	0.69	0.26	0.22
10.0 %-KBF_4	0.62	0.26	0.21
25.0 %-KBF_4	0.72	0.25	0.28

Table 1 Average values of $\cos^2\theta$ for the $[BMIM]^+$ cations in the first layer of cations near positively (a), negatively (b) and neutrally (c) charged graphene walls for mixtures of [BMIM][BF_4] with $LiBF_4$ and KBF_4.

$$A(z) = -kT \cdot \ln\left(\frac{\rho_{Cl}(z)}{\rho_{Cl}(\text{bulk})}\right). \quad (2)$$

We can observe that these curves show oscillations due to the layering behaviour of the IL in the proximities of the wall. Additionally, the height of the barriers impeding the cations of the salt from approaching the walls generally decreases with the amount of salt in the mixtures. Independently of the electrode potential, the highest barriers are found for the lowest concentration of $[Li]^+$ cations, 10%, going from 12 kJ/mol in the neutral wall to 25 kJ/mol in the unfavourable positively charged wall. The values of the free energy barriers near the neutral wall are comparable to that obtained by Smith *et al.*[53] of around 16 kJ/mol for LiFSI doping [EMIM][FSI]. Another remarkable feature is that, as we said previously, both $[Li]^+$ and $[K]^+$ cations can be adsorbed on the negative electrode only at high concentrations of salt due to the occurrence of very high free energy barriers at ca. 0.5 nm that they must overcome for getting to the wall. This is probably due to the dense layer of imidazolium cations that causes a very high energy barrier for the salt cations to approach the negative wall. We get a divergence partly due to the calculation procedure, so the physical barrier is expected to be very high compared to k_BT. Moreover, we can also observe in Fig. 6.b the differences in position and depth of the first minima associated with both cations, that for potassium being deeper than the lithium one, and the displacement of their barriers in Fig. 6.a, which are associated with their different radii.

4 Conclusions

Using MD simulations, we have analyzed the behaviour of mixtures of [BMIM][BF_4] with $LiBF_4$ and KBF_4 confined between two parallel charged and uncharged graphene walls, in order to clarify the potential use of ILs as electrolytes in electrochemical devices. Although for the technical reasons described in the corresponding section the calculations in this

This journal is © The Royal Society of Chemistry [year]

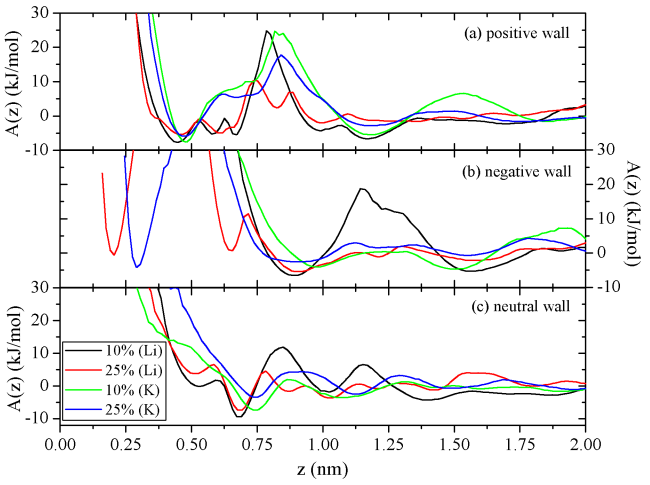

Fig. 6 Free energy profiles for lithium and potassium cations approaching graphene surfaces with positive (a), negative (b) and neutral (c) charge densities for mixtures of [BMIM][BF_4] with $LiBF_4$ and KBF_4.

paper were performed at 450 K, it is expected that our results will also be representative of the behaviour of the systems considered at somewhat lower temperatures. Accordingly, they can be useful for practical applications of those systems; for example, as supercapacitors or batteries.

Number density profiles in the Z direction show, even for the uncharged electrodes, the formation of a layered structure with ion densities higher than in the bulk in the proximities of the surface. This layers were found to be composed of both ionic species of the IL, with the imidazolium cations approximating slightly closer to the electrode. In addition, $[BMIM]^+$ rings within the first layer tend to be oriented in such a way that they form an average angle of around 36° with the wall and, in this case, there are no lithium or potassium cations absorbed on the walls.

As the electrode potential increases, a systematic rearrangement of the ions, in which tetrafluoroborate anions segregate toward the positive electrode and away from the negative wall and imidazolium cations show the opposite behaviour, takes place. In neutral graphene interface, $[BMIM]^+$ cations orient with an average angle of 36° with respect to the normal vector to the surface, and upon charging, they tend to be preferentially oriented in a more perpendicular fashion, forming an average angle of 62° with both the positive and the negative electrode due to the high density of cations screening the negatively charged electrode and the first layer of cations in the positively charged one. Once again, we see the formation of layers near the electrode when the electrode is charged. These layers are formed mainly by cations near the negative electrode and anions near the positive electrode. Oscillations of charge were clearly observed to a depth of 2 nm. Moreover, the fact that we observe the same average angles in the first layer of cations with the negative and the positive electrode shows that the charge of the positive electrode is overcompensated by the layer of anions. This is the result of a delicate balance between screening and packing. We also observed that only for a salt concentration of 25% were $[Li]^+$ and $[K]^+$ able to reach on the negatively charged electrode, but the free energy barriers for these cations approaching the negative wall are considerably higher than $20k_BT$.

Acknowledgement

The authors wish to thank the financial support of Xunta de Galicia through the research projects of references 10-PXIB-103-294 PR, 10-PXIB-206-294 PR and GPC2013-043. Moreover, this work was funded by the Spanish Ministry of Science and Innovation (Grant No. FIS2012-33126). All these research projects are partially supported by FEDER. T. Méndez-Morales thanks the Spanish ministry of Education for her FPU grant. Facilities provided by the Galician Supercomputing Centre (CESGA) are also acknowledged.

References

1 A. Lewandowski and A. Świderska Mocek, *J. Power Sources*, 2009, **194**, 601–609.
2 M. Galiński, A. Lewandowski and I. Stepniak, *Electrochim. Acta*, 2006, **51**, 5567–5580.
3 T. Kuboki, T. Okuyama, T. Ohsaki and N. Takami, *J. Power Sources*, 2005, **26**, 766–769.
4 H. Sakaebe, H. Matsumoto and K. Tatsumi, *Electrochim. Acta*, 2007, **53**, 1048–1054.
5 E. Markevich, V. Baranchugov and D. Aurbach, *Electrochem. Commun.*, 2006, **8**, 1331–1334.
6 M. Egashira, H. Todo, N. Yoshimoto, M. Morita and J. Yamaki, *J. Power Sources*, 2007, **174**, 560–564.
7 V. Borgel, E. Markevich, D. Aurbach, G. Semrau and M. Schmidt, *J. Power Sources*, 2009, **189**, 331–336.
8 T. Méndez-Morales, J. Carrete, S. Bouzón-Capelo, M. Pérez-Rodríguez, O. Cabeza, L. J. Gallego and L. M. Varela, *J. Phys. Chem. B*, 2013, **117**, 3207–3220.
9 S. Menne, J. Pires, M. Anouti and A. Balducci, *Electrochem. Commun.*, 2013, **31**, 39–41.
10 T. Méndez-Morales, J. Carrete, O. Cabeza, O. Russina, A. Triolo, L. J. Gallego and L. M. Varela, *J. Phys. Chem. B*, 2014, **118**, 761–770.
11 E.Frackowiak, *Phys. Chem. Chem. Phys.*, 2007, **9**, 1774–1785.
12 C. Merlet, B. Rotenberg, P. A. Madden, P.-L. Taberna, P. Simon, Y. Gogotsi and M. Salanne, *Nature Materials*, 2012, **11**, 306–310.
13 M. M. Islam, M. T. Alam, T. Okajima and T. Ohsaka, *J. Phys. Chem. C*, 2009, **113**, 3386–3389.
14 V. Lockett, M. Horne, R. Sedev, T. Rodopoulos and J. Ralston, *Phys. Chem. Chem. Phys.*, 2010, **12**, 12499–12512.
15 M. Drüschler, N. Borisenko, J. Wallauer, C. Winter, B. Huber, F. Endres and B. Roling, *Phys. Chem. Chem. Phys.*, 2012, **14**, 5090–5099.
16 R. Costa, C. M. Pereira and F. Silva, *Phys. Chem. Chem. Phys.*, 2010, **12**, 11125–11132.

17 J. Vatamanu, O. Borodin, D. Bedrov and G. D. Smith, *J. Phys. Chem. C*, 2012, **116**, 7940–7951.

18 J. Vatamanu, L. Cao, O. Borodin, D. Bedrov and G. D. Smith, *J. Phys. Chem. Lett.*, 2011, **2**, 2267–2272.

19 C. Merlet, M. Salanne, B. Rotenberg and P. A. Madden, *J. Phys. Chem. C*, 2011, **115**, 16613–16618.

20 M. V. Fedorov and A. A. Kornyshev, *J. Phys. Chem. B*, 2008, **112**, 11868–11872.

21 M. V. Fedorov, N. Georgi and A. A. Kornyshev, *Electrochem. Commun.*, 2010, **12**, 296–299.

22 G. Feng, D. Jiang and P. T. Cummings, *J. Chem. Theory Comput.*, 2012, **8**, 1058–1063.

23 L. Xing, J. Vatamanu, G. D. Smith and D. Bedrov, *J. Phys. Chem. Lett.*, 2012, **3**, 1124–1129.

24 N. Georgi, A. A. Kornyshev and M. V. Fedorov, *J. Electroanal. Chem.*, 2010, **649**, 261–267.

25 M. V. Fedorov and A. A. Kornyshev, *Electrochim. Acta*, 2008, **111**, 6835–6840.

26 D. Jiang, Z. Jin and J. Wu, *Nano Lett.*, 2011, **11**, 5373–5377.

27 A. A. Kornyshev, *J. Phys. Chem. B*, 2007, **111**, 5545–5557.

28 M. Z. Bazant, B. D. Storey and A. A. Kornyshev, *Phys. Rev. Lett.*, 2011, **106**, 046102(1)–046102(4).

29 M. A. Gebbie, M. Valtiner, X. Banquy, E. T. Fox, W. A. Henderson and J. N. Israelachvili, *PNAS*, 2013, **110**, 9674–9679.

30 R. Atkin and G. G. Warr, *J. Phys. Chem. C*, 2007, **111**, 5162–5168.

31 R. Atkin, S. Z. E. Abedin, R. Hayes, L. H. S. Gaspatotto, N. Borisenko and F. Endres, *J. Phys. Chem. C*, 2009, **113**, 13266–13272.

32 R. Atkin, N. Borisenko, M. Drschler, S. Z. E. Abedin, F. Endres, R. Hayes, B. Huber and B. Roling, *Phys. Chem. Chem. Phys.*, 2011, **13**, 6849–6857.

33 D. Wakeham, R. Hayes, G. G. Warr and R. Atkin, *J. Phys. Chem. B*, 2009, **113**, 5961–5966.

34 F. Endres, O. Hofft, N. Borisenko, L. H. Gasparotto, A. Prowald, R. Al-Salman, T. Carstens, R. Atkin, A. Bund and S. Z. E. Abedin, *Phys. Chem. Chem. Phys.*, 2010, **12**, 1724–1732.

35 S. Perkin, L. Crowhurst, H. Niedermeyer, T. Welton, A. M. Smitha and N. N. Gosvami, *Chem. Commun.*, 2011, **47**, 6572–6574.

36 A. M. Smith, K. R. J. Lovelock, N. N. Gosvami, P. Licence, A. Dolan, T. Welton and S. Perkin, *J. Phys. Chem. Lett.*, 2013, **4**, 378–382.

37 M. Mezger, H. Schrder, H. Reichert, S. Schramm, J. S. Okasinski, S. Schder, V. Honkimki, M. Deutsch, B. M. Ocko, J. Ralston, M. Rohwerder, M. Stratmann and H. Dosch, *Science*, 2008, **322**, 424–428.

38 T. Cremer, M. Stark, A. Deyko, H.-P. Steinruck and F. Maier, *Langmuir*, 2011, **27**, 3662–3671.

39 M. Mezger, S. Schramm, H. Schrder, H. Reichert, M. Deutsch, E. J. D. Souza, J. S. Okasinski, B. M. Ocko, V. Honkimki and H. Dosch, *J. Chem. Phys.*, 2009, **131**, 094701(1)–094701(9).

40 S. Baldelli, *Acc. Chem. Res.*, 2008, **41**, 421–431.

41 S. Baldelli, *J. Phys. Chem. Lett.*, 2013, **4**, 244–252.

42 R. S. Payal and S. Balasubramanian, *Chem. Phys. Chem.*, 2012, **13**, 1764–1771.

43 S. A. Kislenko, I. S. Samoylov and R. H. Amirov, *Phys. Chem. Chem. Phys.*, 2009, **11**, 5584–5590.

44 S. Wang, S. Li, Z. Cao and T. Yan, *J. Phys. Chem. C*, 2010, **114**, 990–995.

45 Q. Dou, M. L. Sha, H. Y. Fu and G. Z. Wu, *J. Phys.: Condens. Matter*, 2011, **23**, 175001(1)–175001(8).

46 S. Maolin, Z. Fuchun, W. Guozhong, F. Haiping, W. Chunlei, C. Shimou, Z. Yi and H. Jun, *J. Chem. Phys.*, 2008, **128**, 134504(1)–134504(7).

47 G. Feng, J. S. Zhang and R. Qiao, *J. Phys. Chem. C*, 2009, **113**, 4549–4559.

48 M. Sha, G. Wu, Q. Dou, Z. Tang and H. Fang, *Langmuir*, 2010, **26**, 12667–12672.

49 C. Pinilla, M. G. D. Pópolo, R. M. Lynden-Bell and J. Kohanoff, *J. Phys. Chem. B*, 2005, **109**, 17922–17927.

50 C. Pinilla, M. G. D. Pópolo, J. Kohanoff and R. M. Lynden-Bell, *J. Phys. Chem. B*, 2007, **111**, 4877–4884.

51 M. V. Fedorov and R. M. Lynden-Bell, *Phys. Chem. Chem. Phys.*, 2012, **14**, 2552–2556.

52 R. M. Lynden-Bell, A. I. Frolov and M. V. Fedorov, *Phys. Chem. Chem. Phys.*, 2012, **14**, 2693–2701.

53 G. D. Smith, O. Borodin, S. P. Russo, R. J. Rees and A. F. Hollenkamp, *Phys. Chem. Chem. Phys.*, 2009, **11**, 9884–9897.

54 D. V. D. Spoel, E. Lindahl, B. Hess, A. R. V. Buuren, E. Apol, P. J. Meulenhoff, D. P. Tieleman, A. L. T. M. Sijbers, K. A. Feenstra, R. V. Drunen and H. J. C. Berendsen, *Gromacs User Manual version 4.0*, http://www.Gromacs.org, 2005.

55 W. Humphrey, A. Dalke and K. Schulten, *J. Mol. Graphics*, 1996, **14**, 33–38.

56 W. L. Jorgensen, *J. Phys. Chem.*, 1986, **90**, 1276–1284.

57 S. V. Sambasivarao and O. Acevedo, *J. Chem. Theory Comput.*, 2009, **5**, 1038–1050.

58 C. E. R. Prado and L. C. G. Freitas, *J. Mol. Struct. (Theochem.)*, 2007, **847**, 93–100.

59 T. Yan, S. Li, W. Jiang, X. Gao, B. Xiang and G. A. Voth, *J. Phys. Chem. B*, 2006, **110**, 1800–1806.

60 T. Darden, D. York and L. Pedersen, *J. Chem. Phys.*, 1993, **98**, 10089–10094.

61 I. Yeh and M. L. Berkowitz, *J. Chem. Phys.*, 1999, **111**, 3155–3162.

62 I. Yeh and M. L. Berkowitz, *J. Chem. Phys.*, 2000, **112**, 10491–10495.

63 B. Hess, H. Bekker, H. J. C. Berendsen and J. G. E. M. Fraaije, *J. Comp. Chem.*, 1997, **18**, 1463–1472.

64 B. Hess, *J. Chem. Theory Comp.*, 2007, **4**, 116–122.

65 G. Bussi, D. Donadio and M. Parrinello, *J. Chem. Phys.*, 2007, **126**, 014101(1)–014101(7).

This journal is © The Royal Society of Chemistry [year]

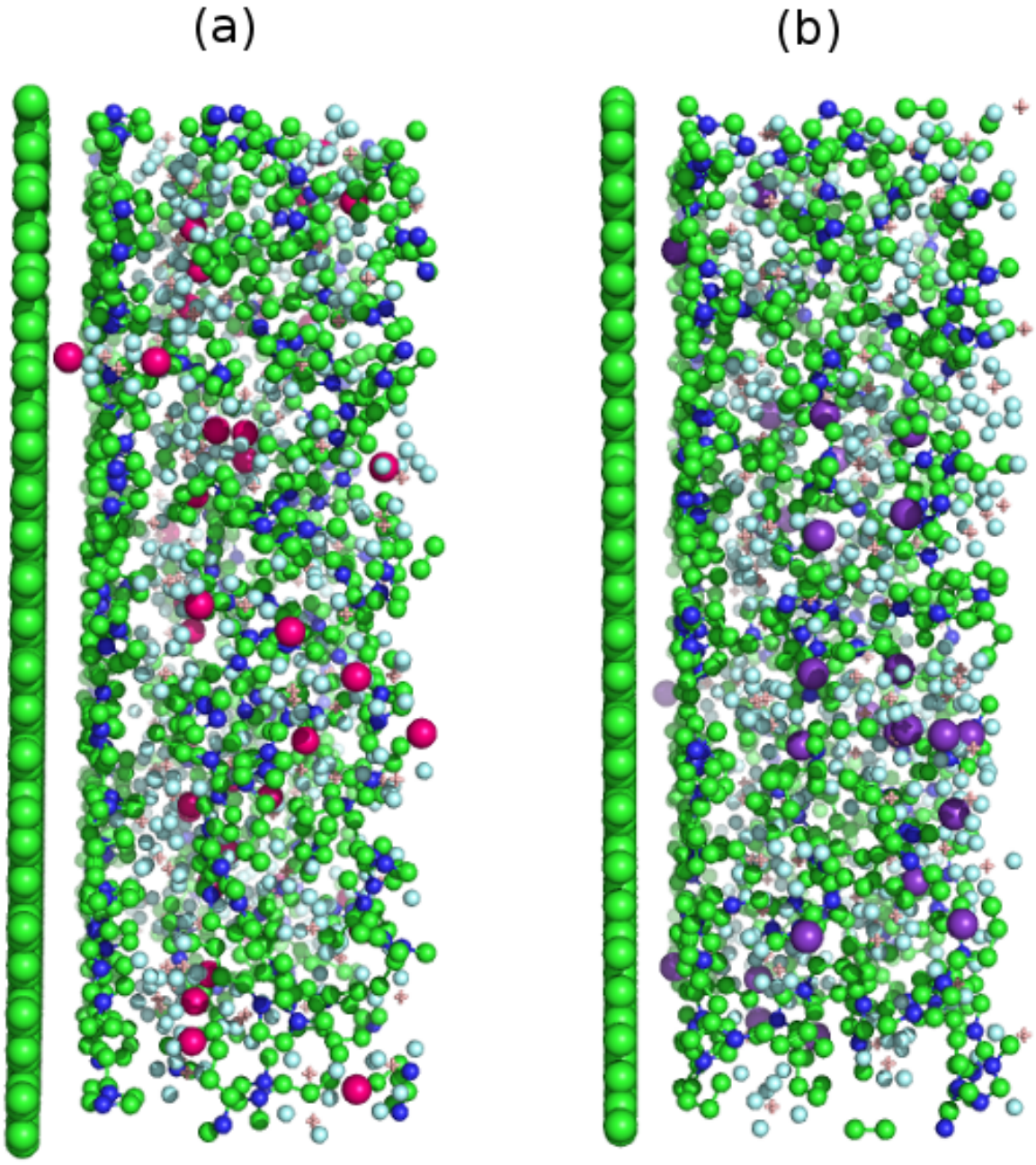
(a)
(b)